S©MR

СИБИРСКИЕ ЭЛЕКТРОННЫЕ
МАТЕМАТИЧЕСКИЕ ИЗВЕСТИЯ
Siberian Electronic Mathematical Reports
http://semr.math.nsc.ru
ISSN 1813-3304

Vol. 20, No. 2, pp. 144–145 (2023)
https://doi.org/10.33048/semi.2023.20.???

УДК 519.6
MSC 76S05,65M06,65M60

ONLINE GENERALIZED MULTISCALE FINITE ELEMENT METHOD FOR MULTICONTINUUM COUPLED FLOW AND TRANSPORT MODEL

D.A. AMMOSOV, J. HUANG
W.T. LEUNG, B. SHAN, M. AL KOBAISI

Communicated by P.P. Petrov

Abstract: In this paper, we present a coupled approach of multicontinuum and multiscale modeling for coupled flow and transport in multiscale porous media. First, we derive a multicontinuum coupled flow and transport model using the multicontinuum homogenization method. For this purpose, we formulate cell problems with constraints, obtain the multicontinuum expansions, and derive the multicontinuum equations. Then, we develop offline and online multiscale approaches based on the Generalized Multiscale Finite Element Method. In the offline approach, we construct multiscale basis functions in

Ammosov D.A., Huang J., Leung W.T., Shan B., and Al Kobaisi M., Online Generalized Multiscale Finite Element Method for Multicontinuum Coupled Flow and Transport Model.

The work of D.A. is supported by the Russian government project Science and Universities (project FSRG-2024-0003) aimed at supporting junior laboratories and the Russian Science Foundation grant 23-71-30013 (https://rscf.ru/project/23-71-30013/).

The work of J.H. was partially supported by the Project for Scientific Research Fund of Hunan Provincial Education Department (22B0138), the Science and Technology Innovation Program of Hunan Province (2024RC3159). J.H. would also like to acknowledge the support of the National Natural Science Foundation of China Project (No. 12071402, No. 12261131501), the Project of Scientific Research Fund of the Hunan Provincial Science and Technology Department (No.2023GK2029, No.2024ZL5017), and Program for Science and Technology Innovative Research Team in Higher Educational Institutions of Hunan Province of China.

Received April, 1, 2024, published August, 23, 2024.

the offline stage by solving local spectral problems. In the online approach, we compute the online basis functions in the online stage by solving local problems based on the residual. The online basis functions allow us to consider the global effects. Numerical results are presented for a model problem with heterogeneous coefficients separable into microscopic and macroscopic parts. The results show the high efficiency of the coupled multicontinuum and multiscale modeling approach. The proposed multiscale methods provide high accuracy with a few degrees of freedom. However, the online approach allows us to accelerate the convergence of the multiscale method significantly.

Keywords: coupled flow and transport, multiscale porous media, multicontinuum homogenization, generalized multiscale finite element method, residual-based online multiscale basis functions.

Аннотация: В данной работе представляется комбинированный подход многоконтинуального и многомасштабного моделирования для связанного потока и переноса в многомасштабных пористых средах. Сначала производится вывод многоконтинуальной модели связанного потока и переноса с помощью метода многоконтинуального усреднения. Для этого формулируются задачи на ячейках с ограничениями, получаются многоконтинуальные разложения и выводятся многоконтинуумные уравнения. Затем разрабатывается офлайн и онлайн многомасштабные подходы, основанные на обобщенном многомасштабном методе конечных элементов. В офлайн подходе многомасштабные базисные функции строятся на офлайн этапе путем решения локальных спектральных задач. В онлайн подходе вычисляются онлайн базисные функции на онлайн этапе путем решения локальные задачи на основе невязки. Онлайн базисные функции позволяют учитывать глобальные эффекты. Численные результаты представлены для модельной задачи с неоднородными коэффициентами, разделяемыми на микроскопическую и макроскопическую части. Результаты показывают высокую эффективность совместного использования многоконтинуального и многомасштабного подходов моделирования. Предложенные многомасштабные методы обеспечивают высокую точность при меньшем количестве степеней свободы. При этом онлайн подход позволяет значительно ускорить сходимость многомасштабного метода.

Ключевые слова: связанный поток и перенос, многомасштабные пористые среды, многоконтинуальное усреднение, обобщенный многомасштабный метод конечных элементов, онлайнмногомасштабные базисные функции на основе невязки.

1 Introduction

Porous media often possess heterogeneous multiscale properties with high contrast. Such features significantly complicate the process of numerical modeling. This paper considers a problem of coupled flow and transport in multiscale porous media. The mathematical model is described by an elliptic equation for pressure and a parabolic convection-diffusion equation for concentration [1]. Among the applications of this model are miscible displacement and oil recovery methods [2].

An accurate numerical solution to such problems requires very fine computational grids to capture all the fine-scale features. However, the resulting discrete systems are huge and have high computational costs. That is why various numerical homogenization and multiscale finite element methods are often used to solve such problems [3, 4, 5]. These methods allow us to solve the problems on a coarse grid with reasonable accuracy. In the numerical homogenization methods, one has to compute effective properties by solving cell problems. In the multiscale finite element methods, one constructs multiscale basis functions to account for the fine-scale features.

However, in the case of complex heterogeneities with high contrast, the standard numerical homogenization and multiscale finite element methods may not give an accurate solution [6, 7] because one macroscopic parameter (effective property or basis function) per macroscopic point may not be sufficient. For such cases, one can use multicontinuum approaches [8, 9, 10]. These approaches distinguish several average states (continua) and introduce several macroscopic parameters, allowing us to consider complex high-contrast heterogeneous media.

Among the new methods of the multicontinuum approaches, one can mention the multicontinuum homogenization method [7, 11, 12]. This method provides a flexible and, at the same time, rigorous procedure for the derivation of multicontinuum equations. For this purpose, cell problems with constraints are formulated to consider various homogenized effects. As a result, we obtain a multicontinuum expansion, which is used to derive multicontinuum equations. This homogenization method has already been successfully applied for various applications [13, 14, 15, 16].

It should be noted that advanced multiscale methods such as the Generalized Multiscale Finite Element Method (GMsFEM) [17] and its variations [18, 19, 20] also can handle complex heterogeneities with high contrast. GMsFEM constructs multiscale basis functions by solving local spectral problems and can set more than one basis function per coarse grid node. However, the resulting macroscopic models are discrete in contrast to the multicontinuum homogenization method.

In this paper, we propose a combined approach of multicontinuum and multiscale modeling. We derive a multicontinuum model of coupled flow and transport using the multicontinuum homogenization method. For this purpose, we formulate cell problems for the flow and transport equations. By

solving these problems, we obtain multicontinuum expansions of pressure and concentration and derive the multicontinuum equations. Next, we develop offline and online multiscale approaches based on GMsFEM to reduce the computational cost further. The offline approach represents a standard procedure in which multiscale basis functions are calculated at the offline stage. In the online approach, we calculate online multiscale basis functions by solving local problems based on the residual while solving the target problem (in the online stage) [19, 22]. The online basis functions allow us to consider global information such as boundary conditions, right-hand sides, and the flow influence on the concentration.

We present numerical results for a particular case of heterogeneous coefficients separable into microscopic and macroscopic parts. Thus, we compute the effective properties based on the microscopic parts and then multiply them by the corresponding macroscopic parts. Next, we perform numerical calculations using the multiscale approaches. The results demonstrate that both approaches can provide an accurate solution. However, the online approach significantly accelerates the convergence of the multiscale method.

The paper is organized as follows. Section 2 presents a brief derivation of the multicontinuum coupled flow and transport model using the multicontinuum homogenization method. In Section 3, we describe the offline multiscale approach based on the Generalized Multiscale Finite Element Method for an efficient solution of the multicontinuum model. Section 4, we present the residual-driven online multiscale approach. In Section 5, we conduct numerical experiments. Finally, Section 6 summarizes our work.

2 Multicontinuum Coupled Flow and Transport Model

In this section, we present a brief derivation of a multicontinuum coupled flow and transport model. One can find a more detailed derivation in [14]. First, let us consider the following mathematical model on a fine scale.

$$\begin{aligned} &-\nabla\cdot(\kappa\nabla p) = g, \quad x\in\Omega,\\ &\phi\frac{\partial c}{\partial t} + u\cdot\nabla c - \nabla\cdot(D\nabla c) = h, \quad x\in\Omega, \quad t\in(0,t_{max}], \end{aligned} \tag{1}$$

where $\Omega\subset\mathbb{R}^2$ is a computational domain, t_{max} is a maximum time, p is a pressure field, c is a concentration field, κ is a heterogeneous permeability coefficient, D is a heterogeneous diffusion coefficient, $u=-\kappa\nabla p$ is the Darcy velocity, and g and h are source/sink terms. Note that κ and D are high-contrast heterogeneous coefficients, i.e., $\frac{\max_{x\in\Omega}\kappa(x)}{\min_{x\in\Omega}\kappa(x)}\gg 1$ and $\frac{\max_{x\in\Omega}D(x)}{\min_{x\in\Omega}D(x)}\gg 1$.

If we supplement these equations with homogeneous Dirichlet boundary conditions and an initial condition for the concentration equation, we can

obtain the following variational formulation

$$\begin{aligned}
&\int_\Omega \kappa \nabla p \cdot \nabla q = \int_\Omega gq, \quad \text{for all } q \in H_0^1(\Omega),\\
&\int_\Omega \phi \frac{\partial c}{\partial t} v + \int_\Omega (u \cdot \nabla c) v + \int_\Omega D \nabla c \cdot \nabla v = \int_\Omega hv, \quad \text{for all } v \in H_0^1(\Omega).
\end{aligned} \tag{2}$$

Next, let us make the following assumptions on our heterogeneous medium. We assume the computational domain Ω is partitioned into coarse blocks K. Also, we suppose that within each K, we have representative volume elements (RVEs) R_K^l capable of representing the whole block in terms of heterogeneity. Note that for some target $R_K^{l_0} = R_K$, we can construct an oversampled RVE R_k^+ by adding other RVEs in layers (see Figure 1). Then, we assume that within each RVE, we can distinguish N regions with different average states, which we call continua. For each of these continua, we define characteristic functions ψ_j $(j = 1, ..., N)$ equal 1 in its continuum and 0 in others.

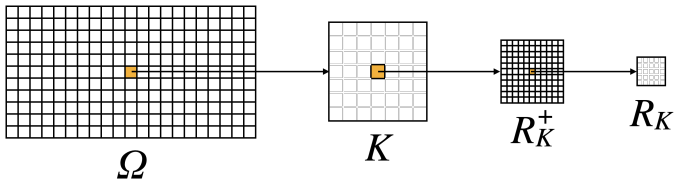

FIG. 1. Schematic illustration of a computational domain Ω, a coarse block K, an oversampled RVE R_K^+, and a RVE R_K

Let us derive the multicontinuum equations for the flow using the multicontinuum homogenization method [7]. For this purpose, we solve cell problems in the oversampled RVE R_K^+ to account for various homogenized effects. The first cell problem is needed to account for gradient effects

$$\begin{aligned}
&\int_{R_K^+} \kappa \nabla \varphi_i^{m,p} \cdot \nabla q - \sum_{j,l} \frac{\beta_{ij}^{ml}}{\int_{R_K^l} \psi_j^l} \int_{R_K^l} \psi_j^l q = 0,\\
&\int_{R_K^l} \varphi_i^{m,p} \psi_j^l = \delta_{ij} \int_{R_K^l} (x_m - \tilde{x}_m) \psi_j^l,\\
&\int_{R_K^{l_0}} (x_m - \tilde{x}_m) \psi_j^{l_0} = 0,
\end{aligned} \tag{3}$$

and the second cell problem considers different averages (constants)

$$\begin{aligned}
&\int_{R_K^+} \kappa \nabla \varphi_i^p \cdot \nabla q - \sum_{j,l} \frac{\beta_{ij}^{l}}{\int_{R_K^l} \psi_j^l} \int_{R_K^l} \psi_j^l q = 0,\\
&\int_{R_K^l} \varphi_i^p \psi_j^l = \delta_{ij} \int_{R_K^l} \psi_j^l.
\end{aligned} \tag{4}$$

After solving these cell problems, we can obtain the following homogenization-like expansions of fine-scale functions over continua in R_K

$$p \approx \varphi_i^p P_i + \varphi_i^{m,p} \nabla_m P_i, \quad q \approx \varphi_s^p Q_s + \varphi_s^{k,p} \nabla_k Q_s, \tag{5}$$

where P_i and Q_s are smooth macroscopic functions that represent the average pressure and concentration of the corresponding continua. Note that we assume Einstein summation convention over repeated indices.

Using the definition of RVE, we can approximate the variational formulation of the flow problem as follows

$$\int_\Omega gq = \int_\Omega \kappa \nabla p \cdot \nabla q = \sum_K \int_K \kappa \nabla p \cdot \nabla q \approx \sum_K \frac{|K|}{|R_K|} \int_{R_K} \kappa \nabla p \cdot \nabla q. \tag{6}$$

Then, we decompose p and q over continua using (5). Note that P_i and Q_s are smooth functions. Therefore, we suppose that their variations and the variations of their gradients are minor compared to the variations of φ_i^p and $\varphi_i^{m,p}$ (according to [7]). As a result, we obtain the following approximation of the variational formulation (see [14] for a more detailed derivation)

$$\begin{aligned} &\int_\Omega \kappa \nabla p \cdot \nabla q \approx \\ &\int_\Omega \widehat{\alpha_{ij}^{mn}} \nabla_m P_i \nabla_n Q_j + \int_\Omega \widehat{\beta_{ij}^m} \nabla_m P_i Q_j + \int_\Omega \widehat{\beta_{ij}^m} P_i \nabla_m Q_j + \int_\Omega \widehat{\beta_{ij}} P_i Q_j, \end{aligned} \tag{7}$$

where $\widehat{\alpha_{ij}^{mn}}$, $\widehat{\beta_{ij}^m}$, and $\widehat{\beta_{ij}}$ are effective properties defined as follows

$$\begin{aligned} \widehat{\alpha_{is}^{mk}} &= \frac{1}{|R_K|} \int_{R_K} \kappa \nabla \varphi_i^{m,p} \cdot \nabla \varphi_s^{k,p}, \\ \widehat{\beta_{ik}^m} = \frac{1}{|R_K|} \int_{R_K} \kappa \nabla \varphi_i^p \cdot \nabla \varphi_k^{m,p}, &\quad \widehat{\beta_{ik}} = \frac{1}{|R_K|} \int_{R_K} \kappa \nabla \varphi_i^p \cdot \nabla \varphi_k^p. \end{aligned} \tag{8}$$

Note that the sum of the second and third terms in (7) is negligible (see [7]). Thus, we obtain the following multicontinuum flow equations (in a strong form)

$$-\nabla_n (\widehat{\alpha_{ij}^{mn}} \nabla_m P_j) + \widehat{\beta_{ij}} P_j = g_i. \tag{9}$$

The multicontinuum transport equations are derived similarly. The cell problems are based on the diffusion term of the transport variational formulation (2). For a more accurate approximation, one can also include the convection term in the cell problems. One can find the detailed derivation of the multicontinuum transport equations in [14].

We obtain the following multicontinuum transport equations

$$\widehat{\gamma_{ij}} \frac{\partial C_j}{\partial t} - \nabla_n (\widehat{\eta_{ij}^{mn}} \nabla_m C_j) + \widehat{\xi_{ij}^m} \nabla_m C_j + \widehat{\Theta_{ij}} C_j = h_i, \tag{10}$$

where the effective properties are defined as follows

$$\widehat{\xi_{ij}^{m}} = P_s\widehat{\chi_{sij}^{m}} + \nabla_l P_s \widehat{\iota_{sij}^{lm}}, \quad \widehat{\Theta_{ij}} = \widehat{\theta_{ij}} + P_s\widehat{\zeta_{sij}} + \nabla_l P_s \widehat{\Upsilon_{sij}^{l}},$$
$$\widehat{\zeta_{sij}} = \frac{1}{|R_K|}\int_{R_K}(-\kappa)(\nabla\varphi_s^p\cdot\nabla\varphi_i^c)\varphi_j^c, \quad \widehat{\eta_{is}^{km}} = \frac{1}{|R_K|}\int_{R_K} D\nabla\varphi_i^{m,c}\cdot\nabla\varphi_s^{k,c},$$
$$\widehat{\chi_{sij}^{m}} = \frac{1}{|R_K|}\int_{R_K}(-\kappa)(\nabla\varphi_s^p\cdot\nabla\varphi_i^{m,c})\varphi_j^c, \quad \widehat{\gamma_{ij}} = \frac{1}{|R_K|}\int_{R_K}\phi\varphi_i^c\varphi_j^c,$$
$$\widehat{\Upsilon_{sij}^{l}} = \frac{1}{|R_K|}\int_{R_K}(-\kappa)(\nabla\varphi_s^{l,p}\cdot\nabla\varphi_i^c)\varphi_j^c, \quad \widehat{\theta_{ik}^{m}} = \frac{1}{|R_K|}\int_{R_K} D\nabla\varphi_i^c\cdot\nabla\varphi_k^{m,c},$$
$$\widehat{\iota_{sij}^{lm}} = \frac{1}{|R_K|}\int_{R_K}(-\kappa)(\nabla\varphi_s^{l,p}\cdot\nabla\varphi_i^{m,c})\varphi_j^c, \quad \widehat{\theta_{ik}} = \frac{1}{|R_K|}\int_{R_K} D\nabla\varphi_i^c\cdot\nabla\varphi_k^c. \tag{11}$$

Finally, we obtain the following multicontinuum coupled flow and transport model

$$-\nabla_n(\widehat{\alpha_{ij}^{mn}}\nabla_m P_j) + \widehat{\beta_{ij}}P_j = g_i, \quad x\in\Omega,$$
$$\widehat{\gamma_{ij}}\frac{\partial C_j}{\partial t} - \nabla_n(\widehat{\eta_{ij}^{mn}}\nabla_m C_j) + \widehat{\xi_{ij}^{m}}\nabla_m C_j + \widehat{\Theta_{ij}}C_j = h_i, \quad x\in\Omega, \quad t\in(0,t_{max}]. \tag{12}$$

We complement this system of equations with the following boundary conditions

$$P_i = 0, \quad C_i = 0, \quad x\in\partial\Omega, \tag{13}$$

and the initial conditions for concentrations

$$C_i|_{t=0} = 0, \quad x\in\Omega. \tag{14}$$

One can apply any appropriate numerical methods to solve this problem. For example, one can use the finite element method with standard piecewise linear basis functions (for spatial approximation) and the backward Euler method (for temporal discretization). However, solving this problem can still present computational challenges in the case of complex heterogeneous media. That is why, in the next sections, we present multiscale model reduction techniques for additional upscaling. This combined approach is also known as a three-level upscaling [21].

3 Generalized Multiscale Finite Element Method

To further reduce the computational cost, we develop an offline multiscale approach based on the Generalized Multiscale Finite Element Method (GMsFEM) [17]. The main idea of this method is to construct multiscale basis functions by solving local spectral problems. One can divide GMsFEM into offline and online stages. We construct a coarse grid and compute multiscale basis functions in the offline stage. In the online stage, we solve the problem on the coarse grid using the computed basis functions.

3.1. Computing multiscale basis functions. Let us introduce a coarse grid $\mathcal{T}^H = \{K_j^H\}_{j=1}^{N_c^H}$, where K_j^H denotes the j-th coarse-grid cell. In GMsFEM, all the computations are performed on local domains. We define a local domain as $\omega_l = \cup\{K_j^H \in \mathcal{T}^H : x_l^H \in \overline{K}_j^H\}$, where x_l^H denotes the l-th coarse-grid node ($l = 1, ..., N_v^H$).

Let us consider the calculation of multiscale basis functions for the multicontinuum flow model. The first step is to construct local snapshot spaces. For $i = 1, ..., N$, $l = 1, ..., N_v^H$, $k = 1, ..., N_v^{\partial\omega_l}$, find $\Phi_{ik}^{snap,l}$ such that

$$\begin{aligned} -\nabla_n(\widehat{\alpha_{ii}^{mn}}\nabla_m\Phi_{ik}^{snap,l}) = 0, \quad x \in \omega_l, \\ \Phi_{ik}^{snap,l} = \delta_k^h, \quad x \in \partial\omega_l, \end{aligned} \tag{15}$$

where $\delta_k^h(x) = \delta_{kr}$ for all $x_k, x_r \in J_h(\omega_l)$, $J_h(\omega_l)$ is a set of all fine-grid nodes on ω_l. Note that, hereafter, we do not use summation over repeated i indices.

After computing all the snapshot functions, we can construct local snapshot spaces for $i = 1, ..., N$ and $l = 1, ..., N_v^H$ as follows

$$W_{P_i}^{snap,l} = \text{span}\{\Phi_{ik}^{snap,l} : k = 1, ..., N_v^{\partial\omega_l}\}.$$

Next, we need to solve local spectral problems in the obtained snapshot spaces. For $i = 1, ..., N$, $l = 1, ..., N_v^H$, find $\Phi_{ik}^l \in W_{P_i}^{snap,l}$ such that

$$\int_{\omega_l} \widehat{\alpha_{ii}^{mn}}\nabla_m\Phi_{ik}^l\nabla_n Q_i = \int_{\omega_l} \lambda_k\tilde{\alpha}_i\Phi_{ik}^l Q_i, \quad \text{for all } Q_i \in W_{P_i}^{snap,l}, \tag{16}$$

where $\tilde{\alpha}_i = \widehat{\alpha_{ii}^{11}}$.

Then, we select M_{off} smallest eigenvalues and their corresponding eigenfunctions. To make our basis functions conforming, we multiply the eigenfunctions by the multiscale partition of unity functions $\Phi_{ik}^{off,l} = \chi_i^l\Phi_{ik}^l$. The multiscale partition of unity functions can be computed as follows. For $i = 1, ..., N$ and each $K_j^H \subset \omega_l$, $l = 1, ..., N_v^H$, find χ_i^l such that

$$\begin{aligned} -\nabla_n(\widehat{\alpha_{ii}^{mn}}\nabla_m\chi_i^l) = 0, \quad x \in K_j^H, \\ \chi_i^l = \mu^l, \quad x \in \partial K_j^H, \end{aligned} \tag{17}$$

where μ^l denotes a standard partition of unity function, which is continuous and linear in ω_l, equal to 1 at x_l^H and 0 at all the other coarse-grid nodes.

Finally, we construct the multiscale spaces for the pressures of each continuum as follows

$$W_{P_i}^{off} = \text{span}\{\Phi_{ik}^{off,l} : 1 \le k \le N_b, \quad 1 \le l \le N_v^H\}. \tag{18}$$

We can construct the multiscale space for $P = (P_1, P_2, ..., P_N)$ as $W_P^{off} = W_{P_1}^{off} \times W_{P_2}^{off} \times ... \times W_{P_N}^{off}$.

The multiscale basis functions for the concentrations are computed in a similar way. All the local problems are based on diffusion terms. At the

end, we obtain the following multiscale spaces for the concentrations of each continuum

$$W_{C_i}^{off} = \text{span}\{\Psi_{ik}^{off,l} : 1 \leq k \leq N_b, \quad 1 \leq l \leq N_v^H\}. \tag{19}$$

Finally, we construct the multiscale space for $C = (C_1, C_2, ..., C_N)$ as $W_C^{off} = W_{C_1}^{off} \times W_{C_2}^{off} \times ... \times W_{C_N}^{off}$.

3.2. Algorithm. Let us perform temporal discretization of the transport problem using the backward Euler method. We denote with N_t a count of time steps and $\tau = t_{max}/N_t$ their size. Then, we obtain the following discrete problems

- *Flow:* Find $P_{ms} = (P_{ms,1}, ..., P_{ms,N}) \in W_P^{off}$ such that

$$b_P(P_{ms}, Q) = L_P(Q), \quad \text{for all } Q \in W_P^{off}, \tag{20}$$

where the bilinear and linear forms are following

$$b_P(P,Q) = \int_\Omega \widehat{\alpha_{ij}^{mn}} \nabla_m P_i \nabla_n Q_j + \int_\Omega \widehat{\beta_{ij}} P_i Q_j, \quad L_P(Q) = \int_\Omega g_j Q_j. \tag{21}$$

- *Transport:* For $k = 1, ..., N_t$, find $C_{ms}^{k+1} = (C_{ms,1}^{k+1}, ..., C_{ms,N}^{k+1}) \in W_C^{off}$ such that

$$s_C(\frac{C_{ms}^k - C_{ms}^{k-1}}{\tau}, V) + b_C(C^k, V) = L_C(V), \quad \text{for all } V \in W_C^{off}, \tag{22}$$

where $C_{ms}^k \approx C_{ms}(t_k)$, $t_k = k\tau$, and the bilinear and linear forms are defined as follows

$$\begin{gathered} b_C(C,V) = \int_\Omega \widehat{\eta_{ij}^{mn}} \nabla_m C_i \nabla_n V_j + \int_\Omega \widehat{\xi_{ij}^m} \nabla_m C_i V_j + \int_\Omega \widehat{\Theta_{ij}} C_i V_j, \\ s_C(C,V) = \int_\Omega \widehat{\gamma_{ij}} C_i V_j, \quad L_C(V) = \int_\Omega h_j V_j. \end{gathered} \tag{23}$$

In practice, one can build the coarse-grid problems by projecting the fine-grid problems using the multiscale projection matrices [17].

4 Online Generalized Multiscale Finite Element Method

This section presents an online multiscale approach based on the Online Generalized Multiscale Finite Element Method (Online GMsFEM). In this approach, we construct additional basis functions by solving local problems based on the residual [19, 22]. The residual allows us to consider the influence of the right-hand side, boundary conditions, and convection terms. Since these basis functions are constructed in the online stage, they are called online multiscale basis functions.

Let us denote with $b_P^l(P,Q)$, $L_P^l(Q)$, $s_C^l(C,V)$, $b_C^l(C,V)$, and $L_C^l(V)$ the corresponding forms from (21) and (23) but with ω_l integration domain

(instead of Ω). Then, we define the following residual forms

$$\begin{aligned} R_P^l(Q;P_{ms}^r) &= L_P^l(Q) - b_P^l(P_{ms}^r, Q), \\ R_C^l(V;C_{ms}^{k,r},C_{ms}^{k-1}) &= L_C^l(V) - s_C^l(\frac{C_{ms}^{k,r}-C_{ms}^{k-1}}{\tau},V) - b_C^l(C^{k,r},V), \end{aligned} \tag{24}$$

where r is an index of online iteration, k is an index of time step, and P_{ms}^r and $C_{ms}^{k,r}$ are the multiscale solutions.

4.1. Multiscale basis functions for the pressures. Let M_{on} be a maximum count of online iterations. Next, set $r = 0$ and $W_P^{ms,r} = W_P^{ms,0} = W_P^{off}$. Then, we obtain the following algorithm for enriching our multiscale space

(1) Solve the global problem for $P_{ms}^r \in W_P^{ms,r}$

$$b_P(P_{ms}^r, Q) = L_P(Q), \quad \text{for all } Q \in W_P^{ms,r}. \tag{25}$$

(2) Solve the local problems for $\Phi_r^{on,l}$ $(l = 1, ..., N_v^H)$ such that

$$b_P^l(\Phi_r^{on,l}, Q) = R_P^l(Q;P_{ms}^r), \quad \text{for all } Q \in W_P^l, \tag{26}$$

where $W_P^l = [H_0^1(\omega_l)]^N$.

(3) Obtain the new multiscale space

$$W_P^{ms,r+1} = W_P^{ms,r} \oplus span\{\Phi_r^{on,l} : 1 \le l \le N_v^H\}, \tag{27}$$

and set $N_{it} = r + 1$.

(4) If $N_{it} >= M_{on}$, set $W_P^{ms} = W_P^{ms,r+1}$ and stop the algorithm; otherwise, let $r = r + 1$ and go to step 1.

Then, we solve the problem (25) in W_P^{ms}.

4.2. Multiscale basis functions for the concentrations. Assume that we are at the k-th time step. Set N_{max} and let $r = 0$ and $W_C^{ms,r} = W_C^{ms,0} = W_C^{off}$. Then, we have the following algorithm

(1) Solve the global problem for $C_{ms}^{r,k} \in W_P^{ms,r}$

$$s_C(\frac{C_{ms}^{k,r}-C_{ms}^{k-1}}{\tau},V) + b_C(C_{ms}^{k,r},V) = L_C(V), \quad \text{for all } V \in W_C^{ms,r}. \tag{28}$$

(2) Solve the local problems for $\Psi_r^{on,l}$ $(l = 1, ..., N_v^H)$ such that

$$s_C^l(\frac{\Psi_r^{on,l}}{\tau},V) + b_C^l(\Psi_r^{on,l},V) = R_C^l(V;C_{ms}^{k,r},C_{ms}^{k-1}), \quad \text{for all } V \in W_C^l, \tag{29}$$

where $W_C^l = [H_0^1(\omega_l)]^N$.

(3) Obtain the new multiscale space

$$W_C^{ms,r+1} = W_C^{ms,r} \oplus span\{\Psi_r^{on,l} : 1 \le l \le N_v^H\}, \tag{30}$$

and set $N_{it} = r + 1$.

(4) If $N_{it} >= M_{on}$, set $W_C^{ms} = W_C^{ms,r+1}$ and stop the algorithm; otherwise, let $r = r + 1$ and go to step 1.

Then, we solve the problem (28) in W_C^{ms} and go to the next time step $k = k + 1$. In practice, we do not need to compute the online basis functions each time step. We can update them with some periodicity (every five or ten time steps).

5 Numerical Results

In this section, we conduct numerical experiments using our combined multicontinuum and multiscale approach. For this purpose, we solve a two-dimensional model problem in a high-contrast heterogeneous medium.

We consider a particular case of separable heterogeneous coefficients. We assume that the coefficients κ and D can be separated into microscopic and macroscopic parts, i.e., $\kappa(x) = \kappa_{mic}(x)\kappa_{mac}(x)$ and $D(x) = D_{mic}(x)D_{mac}(x)$. Next, we suppose that κ_{mac} and D_{mac} are sufficiently smooth functions, and their variations within RVEs are negligible. Moreover, we suppose that κ_{mic} and D_{mic} are periodic and identical over all the RVEs. As a result, we can compute the effective properties based on κ_{mic} and D_{mic} in a small domain region, ignoring κ_{mac} and D_{mac}. Then, multiplying the effective properties by the corresponding macroscopic parts, we get the multicontinuum model (12), for which we use our multiscale model reduction techniques.

We use the open-source computing platform FEniCS for the numerical implementation of the proposed approaches [23]. We visualize the obtained results using the open-source visualization application ParaView [24].

5.1. Effective properties. Let us consider a computational domain $\Omega = [0, 10]\times[0, 10]$. Suppose the microscopic coefficients κ_{mic} and D_{mic} are periodic over the square RVEs R_K^l with size 0.005. We construct an oversampled RVE $R_K^+ = [0, 0.1] \times [0, 0.1]$ by extending a target RVE R_K. Therefore, we have 20×20 RVEs in the oversampled RVE. We discretize each RVE with 10×10 rectangular cells that allow us to capture all the variations of κ_{mic} and D_{mic}.

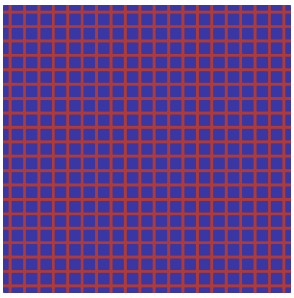

FIG. 2. Microstructure (the first continuum is blue, and the second continuum is red)

In Figure 2, we present the microstructure of the oversampled RVE, where the blue regions correspond to the first continuum, and the red regions correspond to the second continuum. We take $\kappa_{mic} = D_{mic} = 10^{-6}$ in the

first continuum and $\kappa_{mic} = D_{mic} = 1$ in the second continuum. We set constant porosity $\phi = 0.2$ in all the continua. Based on κ_{mic} and D_{mic}, we solve the cell problems and then compute the effective properties (8) and (11). We obtain the following effective properties:

- *Flow*:
  - Diffusion terms: $\widehat{\alpha_{11}^{11}} = \widehat{\alpha_{11}^{22}} = 4.62632 \cdot 10^{-6}$, $\widehat{\alpha_{12}^{11}} = \widehat{\alpha_{12}^{22}} = -2.96803 \cdot 10^{-6}$, $\widehat{\alpha_{21}^{mn}} = \widehat{\alpha_{12}^{mn}}$, $\widehat{\alpha_{22}^{11}} = \widehat{\alpha_{22}^{22}} = 0.218814$, other elements are negligible;
  - Reaction terms: $\widehat{\beta_{11}} = \widehat{\beta_{22}} = 1.19678$ and $\widehat{\beta_{12}} = \widehat{\beta_{21}} = -1.19678$;
- *Transport*:
  - Diffusion and reaction terms: $\widehat{\eta_{ij}^{mn}} = \widehat{\alpha_{ij}^{mn}}$, $\widehat{\theta_{ij}} = \widehat{\beta_{ij}}$;
  - Time derivative terms: $\widehat{\gamma_{11}} = 0.180165$, $\widehat{\gamma_{12}} = \widehat{\gamma_{21}} = -0.0521645$, and $\widehat{\gamma_{22}} = 0.124165$;
  - Flow-related terms:
    - $\widehat{\zeta_{111}} = \widehat{\zeta_{221}} = -0.86706$, $\widehat{\zeta_{112}} = \widehat{\zeta_{222}} = -0.32972$, $\widehat{\zeta_{121}} = \widehat{\zeta_{211}} = 0.86706$, and $\widehat{\zeta_{122}} = \widehat{\zeta_{212}} = 0.32972$;
    - $\widehat{\iota_{222}^{11}} = \widehat{\iota_{222}^{22}} = -0.21881$, other elements lay in the range from $-5.70902 \cdot 10^{-6}$ to $3.85826 \cdot 10^{-6}$;
    - $\widehat{\Upsilon_{sij}^{l}}$ and $\widehat{\chi_{sij}^{m}}$ lay in the range from $-5.82823 \cdot 10^{-10}$ to $5.82823 \cdot 10^{-10}$.

5.2. Multiscale modeling. To obtain the heterogeneous coefficients given over the whole Ω, we need to multiply the computed effective properties by the corresponding macroscopic parts. We present the macroscopic parts of κ and D in Figure 3.

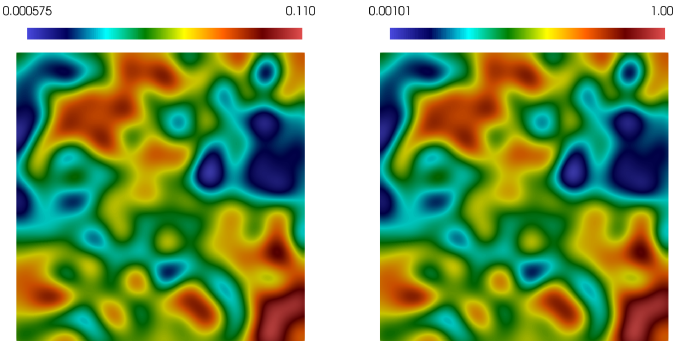

FIG. 3. Distributions of κ_{mac} and D_{mac} (from left to right)

For a fine grid, we use a uniform grid with $2 \times 160 \times 160$ triangular cells and 25921 vertices that can capture all the variations of the heterogeneous coefficients. We use a uniform coarse grid with 10×10 rectangular cells and 121 vertices for our multiscale approaches.

We set the initial conditions (14) and the boundary conditions (13). We simulate for $t_{max} = 600$ using 40 time steps. For the flow and transport

source terms, we take $g_i = \vartheta_i \bar{g}$ and $h_i = \vartheta_i \bar{h}$ $(i = 1, 2)$, where $\vartheta_1 = 0.64$, $\vartheta_2 = 0.36$, and $\bar{g}$ and $\bar{h}$ are following

$$\bar{g} = g_0 \exp\left(-(x_1/L)^2\right), \quad \bar{h} = h_0 \exp\left(-\frac{(x_1/L - x_1^{in})^2 + (x_2/L - x_2^{in})^2}{2\sigma^2}\right).$$

Here, we set $g_0 = 1.9 \cdot 10^{-4}$, $h_0 = 1.4 \cdot 10^{-3}$, $(x_1^{in}, x_2^{in}) = (0.5, 0.5)$, $L = 10$, and $\sigma = 0.11$.

We consider both offline and online multiscale approaches on a coarse grid. As a reference solution method, we consider a finite element method with standard piecewise linear basis functions on a fine grid. We use the following relative L_2 and energy error norms to compare the multiscale solutions with the reference solution.

$$e_{L_2}^{P_i} = \sqrt{\frac{\int_\Omega (P_i^{ref} - P_i^{ms})^2 dx}{\int_\Omega (P_i^{ref})^2 dx}}, \quad e_a^P = \sqrt{\frac{a_P(P^{ref} - P^{ms}, P^{ref} - P^{ms})}{a_P(P^{ref}, P^{ref})}},$$

$$e_{L_2}^{C_i} = \sqrt{\frac{\int_\Omega (C_i^{ref} - C_i^{ms})^2 dx}{\int_\Omega (C_i^{ref})^2 dx}}, \quad e_a^C = \sqrt{\frac{a_C(C^{ref} - C^{ms}, C^{ref} - C^{ms})}{a_C(C^{ref}, C^{ref})}},$$

where the superscript ref indicates the reference solution, and the superscript ms corresponds to the multiscale solution. We use the forms $a_P(P, Q) = b_P(P, Q)$ and $a_C(C, V) = s_C(\frac{C}{\tau}, V) + b_C(C, V)$ to compute the energy error.

In Figure 4, we present distributions of the first and second continuum pressures and the first and second continuum concentrations at the final time (from left to right). Figure 4a depicts the reference solution on a fine grid. Figures 4b and 4c represent multiscale solutions using four offline basis functions combined with two and one online basis functions, respectively. Figure 4d depicts the multiscale solution using four offline basis functions.

One can see that the multiscale solution without online basis functions differs from the reference solution. It is especially noticeable in the first continuum pressure distribution. There are also some differences in the other fields. Adding one online basis function improves the accuracy of the solution. One can notice only slight errors near the left boundary for the first continuum pressure distribution. When two online basis functions are applied, the multiscale solution becomes almost identical to the reference solution. Thus, we see that online basis functions can significantly improve the accuracy of the multiscale solution.

Table 1 presents the relative L_2 and energy errors for different numbers of offline and online basis functions. One can see that increasing the number of offline basis functions leads to decreasing errors. For example, the energy errors of pressures and concentrations with one offline basis function are 29.3% and 12.4%, respectively. At the same time, using eight offline basis functions, the energy errors of pressures and concentrations are 3.61% and 0.93%, respectively.

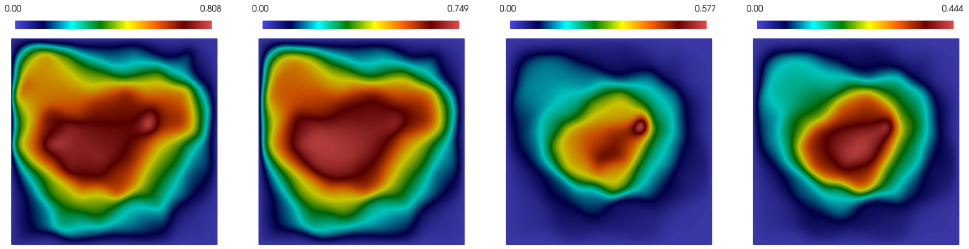

(A) Reference solution

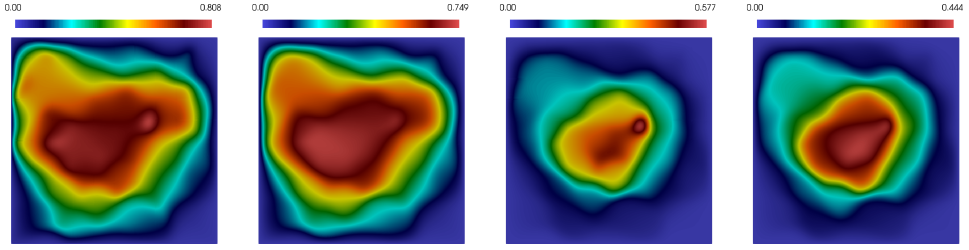

(B) Multiscale solution using two online and four offline basis functions

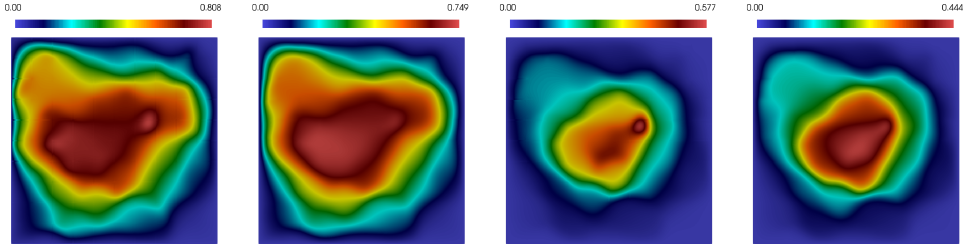

(C) Multiscale solution using one online and four offline basis functions

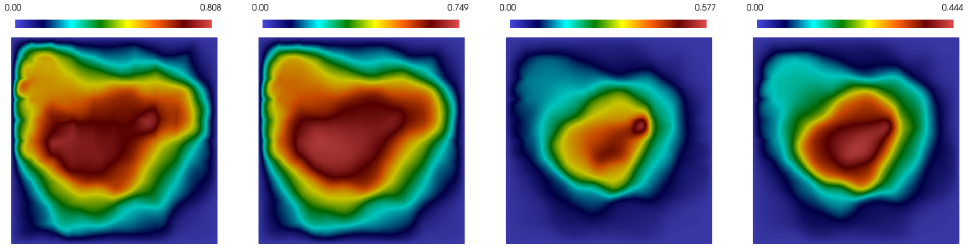

(D) Multiscale solution using four offline basis functions

FIG. 4. Distributions of P_1, P_2, C_1, and C_2 at the final time (from left to right)

Online basis functions significantly improve the accuracy of the multiscale solution. For example, if we add one online basis function to two offline basis functions, the energy error of pressures drops from 24.8% to 5.79%, and the energy error of concentrations drops from 7.23% to 1.72%. When we add the second online basis function, the energy errors become less than 1% for both pressures and concentrations.

TABLE 1. Relative L_2 and energy errors of the multiscale method for flow and transport problems (at the final time) using different numbers of offline and online basis functions. The fine-grid problems' size is 51842.

M_{on}	DOF	Flow			Transport		
		$e_{L_2}^{P_1}$	$e_{L_2}^{P_2}$	e_a^P	$e_{L_2}^{C_1}$	$e_{L_2}^{C_2}$	e_a^C
$M_{off} = 1$							
0	242	1.01e-01	8.38e-02	2.93e-01	9.88e-02	8.10e-02	1.24e-01
1	484	1.31e-02	9.88e-03	7.45e-02	2.07e-02	8.84e-03	2.81e-02
2	726	1.65e-03	6.46e-04	1.09e-02	1.30e-02	2.31e-03	1.33e-02
$M_{off} = 2$							
0	484	7.43e-02	6.33e-02	2.48e-01	5.04e-02	4.26e-02	7.23e-02
1	726	9.37e-03	5.90e-03	5.79e-02	1.24e-02	4.15e-03	1.72e-02
2	968	1.26e-03	4.89e-04	9.67e-03	9.84e-03	1.42e-03	9.86e-03
$M_{off} = 4$							
0	968	2.71e-02	1.87e-02	1.17e-01	1.54e-02	1.37e-02	2.89e-02
1	1210	4.34e-03	2.88e-03	3.20e-02	5.36e-03	3.00e-03	9.25e-03
2	1452	1.34e-03	1.05e-03	1.35e-02	3.48e-03	8.96e-04	4.30e-03
$M_{off} = 8$							
0	1936	9.59e-03	1.62e-03	3.61e-02	4.19e-03	2.01e-03	9.34e-03
1	2178	1.11e-03	3.87e-04	8.14e-03	1.79e-03	4.25e-04	2.94e-03
2	2420	2.69e-04	1.14e-04	2.57e-03	1.56e-03	1.21e-04	1.65e-03

Thus, the application of online basis functions can significantly improve the accuracy of the multiscale solution. The offline multiscale approach can also provide an accurate solution, but it requires more multiscale basis functions per coarse-grid node. Therefore, the online multiscale approach accelerates the convergence of the multiscale method.

6 Conclusion

In this paper, we have proposed a combined multicontinuum and multiscale modeling approach to solve the coupled flow and transport problem. First, we have employed the multicontinuum homogenization method to obtain a multicontinuum macroscopic model. Then, we have presented offline and online multiscale approaches based on the Generalized Multiscale Finite Element Method for further upscaling. The offline approach is the standard GMsFEM procedure, in which the multiscale basis functions are computed in an offline stage. In the online approach, we compute the online multiscale basis functions by solving local problems based on the residual. These basis functions allow us to consider global effects and accelerate the convergence.

We have presented numerical results for the case with heterogeneous coefficients separable into microscopic and macroscopic parts. We have solved the cell

problems and computed the effective properties based on the microscopic parts, assuming that the variations of the macroscopic parts are negligible. Multiplying with the corresponding macroscopic parts, we have obtained the effective properties over the whole domain. Then, we have performed computations using the proposed multiscale approaches. The results demonstrate that both methods can provide an accurate solution. However, the offline approach needs more multiscale basis functions per coarse-grid node to account for all the solution's features. The online approach can achieve high accuracy with fewer degrees of freedom, accelerating the convergence of the multiscale method.

References

[1] E.T. Chung, Y. Efendiev, W.T. Leung, and J. Ren, *Multiscale simulations for coupled flow and transport using the generalized multiscale finite element method*, Computation, **3**:4 (2015), 670–686.

[2] C. Zhu, J.J. Sheng, A. Ettehadtavakkol, Y. Li, H. Gong, Z. Li, and M. Dong, *Numerical and experimental study of enhanced shale-oil recovery by CO2 miscible displacement with NMR*, Energy & Fuels, **34**:2 (2020), 1524–1536.

[3] Y. Amanbek, G. Singh, M.F. Wheeler, and H. van Duijn, *Adaptive numerical homogenization for upscaling single phase flow and transport*, Journal of Computational Physics, **387** (2019), 117–133.

[4] A. Talonov, and M. Vasilyeva, *On numerical homogenization of shale gas transport*, Journal of Computational and Applied Mathematics, **301** (2016), 44–52.

[5] Y. Efendiev, and T. Y. Hou, *Multiscale finite element methods: theory and applications*, Springer Science & Business Media, **4** (2009).

[6] Y. Efendiev, J. Galvis, and X.-H. Wu, *Multiscale finite element methods for high-contrast problems using local spectral basis functions*, Journal of Computational Physics, **230**:4 (2011), 937–955.

[7] Y. Efendiev, and W.T. Leung, *Multicontinuum homogenization and its relation to nonlocal multicontinuum theories*, Journal of Computational Physics, **474** (2023), 111761.

[8] L.I. Rubinštein, *On a question about the propagation of heat in heterogeneous media*, Izvestiya Akad Nauk SSSR. Ser. Geograf. Geofiz, **12** (1948), 27–45.

[9] G.I. Barenblatt, I.P. Zheltov, and I.N. Kochina, *Basic concepts in the theory of seepage of homogeneous liquids in fissured rocks [strata]*, Journal of applied mathematics and mechanics, **24**:5 (1960), 1286–1303.

[10] T. Arbogast, J. Douglas Jr., and U. Hornung, *Derivation of the double porosity model of single phase flow via homogenization theory*, SIAM Journal on Mathematical Analysis, **21**:4 (1990), 823–836.

[11] E. Chung, Y. Efendiev, J. Galvis, and W.T. Leung, *Multicontinuum homogenization. General theory and applications*, Journal of Computational Physics, **510** (2024), 112980.

[12] W.T. Leung, *Some convergence analysis for multicontinuum homogenization*, arXiv preprint arXiv:2401.12799 (2024).

[13] W. Xie, Y. Efendiev, Y. Huang, W.T. Leung, and Y. Yang, *Multicontinuum homogenization in perforated domains*, arXiv preprint arXiv:2404.17471 (2024).

[14] D. Ammosov, W.T. Leung, B. Shan, and J. Huang, *Multicontinuum Homogenization for Coupled Flow and Transport Equations*, arXiv preprint arXiv:2405.14572 (2024).

[15] U. Kalachikova, and D. Ammosov, *Advancing wave equation analysis in dual-continuum systems: A partial learning approach with discrete empirical interpolation and deep neural networks*, Journal of Computational and Applied Mathematics, **443**, 115755 (2024).
[16] D. Ammosov, S. Stepanov, D. Spiridonov, and W. Li, *Multicontinuum homogenization for Richards' equation: The derivation and numerical experiments*, Russian Journal of Numerical Analysis and Mathematical Modelling, **38**:4 (2023), 207–218.
[17] Y. Efendiev, J. Galvis, and T.Y. Hou, *Generalized multiscale finite element methods (GMsFEM)*, Journal of computational physics, **251** (2013), 116–135.
[18] E. T. Chung, Y. Efendiev, and C. S. Lee, *Mixed generalized multiscale finite element methods and applications*, Multiscale Modeling & Simulation, **13**:1 (2015), 338–366.
[19] E.T. Chung, Y. Efendiev, and W.T. Leung, *Residual-driven online generalized multiscale finite element methods*, Journal of Computational Physics, **302** (2015), 176–190.
[20] E.T. Chung, Y. Efendiev, and W.T. Leung, *Constraint energy minimizing generalized multiscale finite element method*, Computer Methods in Applied Mechanics and Engineering, **339** (2018), 298–319.
[21] M. Vasilyeva , E.T. Chung, Y. Efendiev, and A. Tyrylgin, A Three-Level Multi-Continua Upscaling Method for Flow Problems in Fractured Porous Media, Communications in Computational Physics, **27**:2 (2019), 619–638.
[22] D. Ammosov, T. Mai, and J. Galvis, *Generalized multiscale finite element method for a nonlinear elastic strain-limiting Cosserat model*, Journal of Computational Physics, **519** (2024), 113428.
[23] A. Logg, K.-A. Mardal, and G. Wells, *Automated solution of differential equations by the finite element method: The FEniCS book*, Springer Science & Business Media, **84**, 2012.
[24] J. Ahrens, B. Geveci, and C. Law, *Paraview: An end-user tool for large data visualization*, The visualization handbook, **717**:8 (2005), 717–731.

Ammosov Dmitry Andreevich
Chemical and Petroleum Engineering Department,
Khalifa University of Science and Technology, Abu Dhabi, 127788, UAE
Laboratory of Computational Technologies and Artificial Intelligence,
North-Eastern Federal University, Belinsky st., 58,
677000, Yakutsk, Russia
Email address: dmitrii.ammosov@ku.ac.ae, dmitryammosov@gmail.com

Huang Jian
School of Mathematics and Computational Science, Xiangtan University,
National Center for Applied Mathematics in Hunan and
Hunan Key Laboratory for Computation and Simulation in
Science and Engineering, Xiangtan 411105, Hunan, China
Email address: huangjian213@xtu.edu.cn

Leung Wing Tat
Department of Mathematics, City University of Hong Kong, Hong Kong
Email address: wtleung27@cityu.edu.hk

Shan Buzheng
Department of Mathematics, Texas A&M University,
College Station, TX 77843, USA
Email address: shanbzh@tamu.edu

Al Kobaisi Mohammed
Chemical and Petroleum Engineering Department,
Khalifa University of Science and Technology, Abu Dhabi, 127788, UAE
Email address: mohammed.alkobaisi@ku.ac.ae